Smart Structures and Systems, Vol. 4, No. 5 (2008) 667-684
DOI: http://dx.doi.org/10.12989/sss.2008.4.5.667

Real-time large-scale hybrid testing for seismic performance evaluation of smart structures

Oya Mercan*, James Ricles‡, Richard Sause‡† and Thomas Marullo‡‡

Department of Civil and Environmental Engineering, Lehigh University, 117 ATLSS Drive, Bethlehem, PA 18015, USA

(Received April 5, 2007, Accpeted December 11, 2007)

Abstract. Numerous devices exist for reducing or eliminating seismic damage to structures. These include passive dampers, semi-active dampers, and active control devices. The performance of structural systems with these devices has often been evaluated using numerical simulations. Experiments on structural systems with these devices, particularly at large-scale, are lacking. This paper describes a real-time hybrid testing facility that has been developed at the Lehigh University NEES Equipment Site. The facility enables real-time large-scale experiments to be performed on structural systems with rate-dependent devices, thereby permitting a more complete evaluation of the seismic performance of the devices and their effectiveness in seismic hazard reduction. The hardware and integrated control architecture for hybrid testing developed at the facility are presented. An application involving the use of passive elastomeric dampers in a three story moment resisting frame subjected to earthquake ground motions is presented. The experiment focused on a test structure consisting of the damper and diagonal bracing, which was coupled to a nonlinear analytical model of the remaining part of the structure (i.e., the moment resisting frame). A tracking indictor is used to track the actuator's ability to achieve the command displacement during a test, enabling the quality of the test results to be assessed. An extension of the testbed to the real-time hybrid testing of smart structures with semi-active dampers is described.

Keywords: real-time hybrid testing; performance evaluation; elastomeric damper; seismic hazard reduction; servo-hydraulic control.

1. Introduction

Numerous devices have been developed for seismic hazard mitigation of structures and mitigation of other types of dynamic structural response. These devices include passive dampers, semi-active dampers, and active control devices. To develop an understanding of the effectiveness of the use of these devices towards reducing seismic damage in structures, testing of the devices in conjunction with the structural system is required. Because these devices are typically sensitive to loading rate, the tests must be performed in real time (i.e. at the loading rate that occurs in a real structure under dynamic loading).

Real-time hybrid testing is an experimental technique for investigating the dynamic behavior of

*Post-Doctoral Researcher/Adjunct Faculty
‡Bruce G. Johnston Professor, E-mail: jmr5@lehigh.edu
‡†Joseph T. Stuart Professor of Structural Engineering
‡‡Research Scientist

complex structures. Hybrid testing combines physical testing with numerical simulation (Dermitzakis and Mahin 1985), and provides a viable alternative for dynamic testing of structural systems. The structure to be tested is divided into a physical component (test structure) and a numerical model (analytical substructure). The analytical substructure includes the mass of the structure (lumped at discrete locations), and the inherent structural damping. During the test, the displacement response of the structure is calculated using time step integration of the equations of motion. The displacements are imposed on the test structure using actuators and to the analytical substructure at the discrete locations where lumped masses are assumed. The forces required to produce these displacements in the test structure and analytical substructure are measured and computed, respectively, and fed back to the simulation to calculate the command displacements corresponding to the next time step.

In real-time hybrid testing the displacements are imposed in real time, thus allowing testing of systems with rate-dependent components (Nakashima, *et al.* 1992, Nakashima and Masaoka 1999, Darby, *et al.* 2001, Shing *et al*. 2004, Mercan and Ricles 2005, Mercan and Ricles 2007, Mercan 2007). Real-time hybrid testing makes it possible to properly test devices for seismic response control, including passive, semi-active, and active control devices, which are typically nonlinear and rate-dependent. Through the use of real-time hybrid testing, the interaction of these devices with the structural system during a seismic event is accounted for, enabling realistic demands to be imposed on the devices.

The Real-time Multi-directional (RTMD) Earthquake Simulation Facility at Lehigh University is an equipment site within the Network for Earthquake Engineering Simulation (NEES). NEES is a program sponsored by the National Science Foundation (NSF) which established a new generation of experimental facilities for earthquake engineering. The RTMD facility enables multi-directional real-time seismic testing of large-scale structural components, structural subassemblages, and superassemblages (systems). The integration of the capabilities of the RTMD earthquake simulation facility with analytical research enables the seismic design and performance of the civil and mechanical infrastructure systems in the U.S. to be significantly advanced. The integration of experimental and analytical research occurs in two ways: (1) real-time hybrid testing is conducted, where parts of a structural system are simulated using analytical models and coupled to either one, or multiple test structures to simulate real earthquake forces on the complete structural system; and (2) information from the experiments is acquired, archived, and disseminated in a form that enables evaluation of existing or the development of new analytical models, material constitutive relationships, performance-based design procedures, and devices that reduce seismic hazards in structural systems. Support from high quality experimental data is essential to gain acceptance of new analysis and design methods.

2. NEES RTMD facility

The RTMD earthquake simulation facility is housed in the Multi-directional Experimental Laboratory at the ATLSS Engineering Research Center, Lehigh University (see Fig. 1). The ATLSS Laboratory has a strong floor that measures 31.1 m × 15.2 m in plan, and a multi-directional reaction wall that measures up to 15.2 m in height. Anchor points are spaced on a 1.5-m grid along the floor and walls. Each anchor point can resist 1.33 MN tension force and 2.22 MN shear force. Additional steel framing is used in combination with the strong floor and reaction walls to create a wide variety of test configurations.

To create the RTMD earthquake simulation facility, several pieces of equipment have been installed in the ATLSS Laboratory. This equipment includes five dynamic, double-rodded hydraulic actuators with

Fig. 1 ATLSS laboratory multidirectional reaction wall at the RTMD Facility

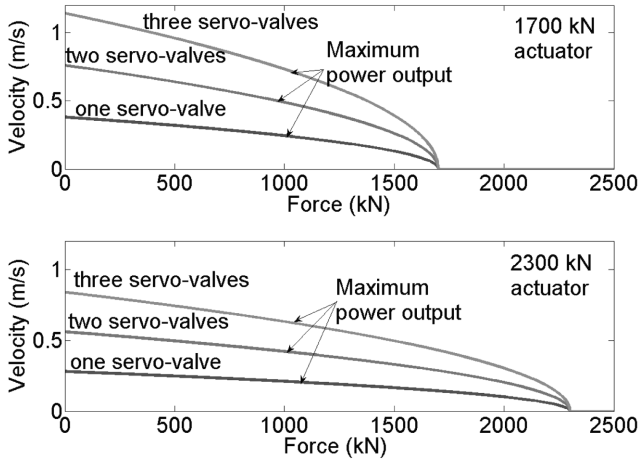

Fig. 2 RTMD facility actuator hydraulic power curves

a +/-500 mm stroke. Two of these actuators have a 2300 kN maximum load capacity, and the remaining three actuators have 1700 kN maximum load capacity. Each of the actuators is ported for three 1500 liter/min servo-valves, enabling them to achieve a maximum nominal velocity of 840 mm/sec (2300 kN actuators) and 1140 mm/sec (1700 kN actuators). The hydraulic power curves for these actuators are shown in Fig. 2.

The existing hydraulic power supply system at ATLSS consisted of five 2250 liter/min pumps. A hydraulic oil reserve and two banks of accumulators were added to enable strong ground motion effects to be sustained for up to 30 seconds. The accumulators supply a total accumulated oil volume of 3030 liters.

The servo-hydraulic integrated control system architecture for the RTMD earthquake simulation facility is shown in Fig. 3. An 8-channel digital controller (identified as the Real-time Control Workstation in Fig. 3), with a 1024 Hz clock speed, controls the motion of the actuators through a closed servo-control loop. The Real-time Control Workstation is integrated with the Simulation Workstation, Real-Time Target Workstation and Data Acquisition Mainframe, as well as the Telepresence Server using SCRAMNet. SCRAMNet is a fiber optic communication device that enables shared memory and time synchronization to the Control or Target Workstations. The Target Workstation communicates with the

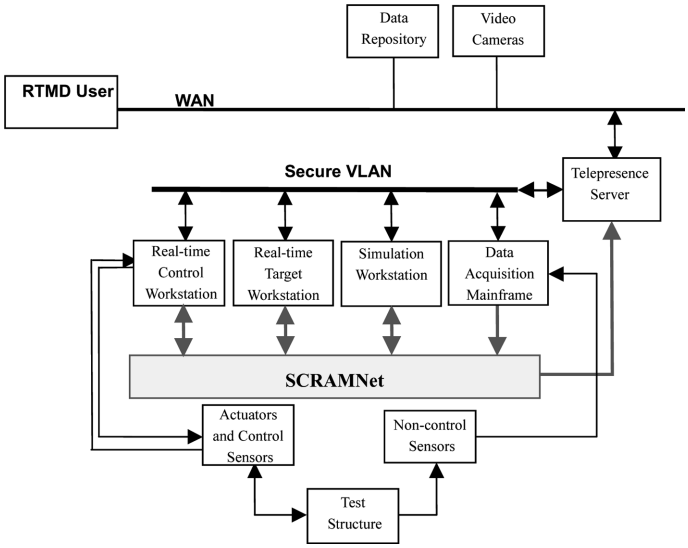

Fig. 3 RTMD earthquake simulation facility integrated control system architecture

Control Workstation and Data Acquisition Mainframe using SCRAMNet, thereby providing a single synchronization source for experiments. The Data Acquisition Workstation controls a high speed 256-channel data acquisition mainframe capable of acquiring data at 1024 Hz per channel. The integrated control system configuration permits complex testing algorithms, servo-hydraulic control laws, and analytical substructures to be developed on the Simulation Workstation and downloaded on to the Target Workstation. The latter is used for hybrid testing. The Target Workstation runs Mathworks xPC Target software. The testing algorithms and any new servo-control laws are developed using SIMULINK (2007), compiled on the Simulation Workstation and downloaded to the Target Workstation. Command signals for imposing displacements on a test structure are generated on the Target Workstation by the integration algorithm, where complex analytical models can reside (e.g. MATLAB or SIMULINK) for integrating the equations of motion in conjunction with the test structure for real-time hybrid testing. Feedback signals needed to determine the command signal for the next time step during a test are acquired from the Control Workstation and the Data Acquisition Mainframe (e.g. the measured actuator forces and current position of the test structure to enable kinematic compensation for multi-directional real-time pseudo-dynamic tests). Through the use of SCRAMNet and a synchronization procedure tied to the clock speed of the controller, where the Control Workstation performs a read-write-execute sequence while the Target Workstation performs a read-execute-write sequence, along with the Data Acquisition pushing sensor data, the communication delay between the systems is equal to one-clock tick of the controller speed, which equals 1/1024 sec.

The integrated control system promotes teleobservation through a Telepresence Server which links networked digital video and synchronized SCRAMNet data. The digital video is acquired from pan-tilt-zoom web cameras and fixed position cameras that are controlled through a user interface on the Telepresence Server. Live video feeds are shared with remote users through FlexTPS (NEES 2007a). FlexTPS is a software system designed to enable the remote viewing and robotic control of video via a web browser. Experimental data and digital video is acquired and synchronously archived from the SCRAMNet through Data Turbine (NEES 2007b). Data Turbine provides high performance time-

synchronized data streaming services for both static and dynamic data. Remote users can view live and archived Data Turbine sources through RDV (NEES 2007c). RDV (the Real-time Data Viewer) provides an interface for viewing real-time, synchronzied, streaming data from an equipment site.

Prior to conducting a test, the task of passing metadata to and from each workstation is performed using a secure VLAN connection. As an alternative to using the Target Workstation as explained above, the Digital Signal Processor (DSP) in the Control Workstation can be programmed with new servo-hydraulic control laws as well as real-time testing algorithms. This approach for testing is, however, limited by the computational capacity of the DSP.

3. RTMD real-time hybrid testing algorithm

The algorithm used at the RTMD facility to integrate the equations of motion is based on the Hilber a-method (Hilber, *et al*. 1977). The α-method is an implicit integration algorithm, and is shown below:

$$\mathbf{M}\mathbf{a}_{i+1} + (1+\alpha)\mathbf{C}\mathbf{v}_{i+1} - \alpha\mathbf{C}\mathbf{v}_i + (1+\alpha)\mathbf{r}_{i+1} - \alpha\mathbf{r}_i = (1+\alpha)\mathbf{P}_{i+1} - \alpha\mathbf{P}_i \tag{1}$$

$$\mathbf{d}_{i+1} = \mathbf{d}_i + \Delta t\mathbf{v}_i + (\Delta t)^2[(0.5-\beta)\mathbf{a}_i + \beta\mathbf{a}_{i+1}] \tag{2}$$

$$\mathbf{v}_{i+1} = \mathbf{v}_i + \Delta t[(1-\gamma)\mathbf{a}_i + \gamma\mathbf{a}_{i+1}] \tag{3}$$

Eq. (1) presents the equations of motion, where **M**, **C**, **r**, and **P** are equal to the mass matrix, viscous damping matrix, total restoring force vector, and load vector, respectively, and i and i+1 are associated with the time step. The Newmark direct integration equations (Newmark 1959) are used in Eq. (2) to relate the displacements $\mathbf{d}_{i+1}$ at time step i+1 to the displacements $\mathbf{d}_i$, velocities $\mathbf{v}_i$, and accelerations $\mathbf{a}_i$ at time step i, along with the accelerations $\mathbf{a}_{i+1}$ at time step i+1, and in Eq. (3) the velocities $\mathbf{v}_{i+1}$ at time step i+1 to the velocities $\mathbf{v}_i$ and accelerations $\mathbf{a}_i$ at time step i, along with the accelerations $\mathbf{a}_{i+1}$ at time step i+1. In the above equations Δt is the time step size and α, β and γ are integration constants. To attain unconditional stability and a favorable energy-dissipation property, it is recommended (Hilber, *et al*. 1977) to use $\beta = (1-\alpha)^2/4$ and $\gamma = 1/2-\alpha$, with $-1/3 \le \alpha \le 0$. If $\mathbf{v}_{i+1}$ from Eq. (3) is substituted into the equilibrium equations, the accelerations $\mathbf{a}_{i+1}$ (i.e., at the end of current time step) are obtained, and the displacements $\mathbf{d}_{i+1}$ from Eq. (2) are equal to:

$$\mathbf{d}_{i+1} = \mathbf{d}_i + \Delta t\mathbf{v}_i + (\Delta t)^2(0.5-\beta)\mathbf{a}_i +$$

$$(\Delta t)^2\beta\overline{\mathbf{M}}^{-1}[(1+\alpha)\mathbf{P}_{i+1} - \alpha\mathbf{P}_i - \mathbf{C}\mathbf{v}_i - (1+\alpha)(1-\gamma)\mathbf{C}\Delta t\mathbf{a}_i - (1+\alpha)\mathbf{r}_{i+1} + \alpha\mathbf{r}_i] \tag{4}$$

where $\overline{\mathbf{M}} = (\mathbf{M} + (1+\alpha)\gamma\mathbf{C}\Delta t)$. To calculate the displacements $\mathbf{d}_{i+1}$ at the next time step (i +1) using Eq. (4), the current time step information ($\mathbf{d}_i$, $\mathbf{v}_i$, $\mathbf{a}_i$, $\mathbf{r}_i$, and $\mathbf{P}_i$) and next time step information ($\mathbf{r}_{i+1}$ and $\mathbf{P}_{i+1}$) are required. The externally applied loads **P** are known. However, $\mathbf{r}_{i+1}$ depends on reaching the displacements $\mathbf{d}_{i+1}$ and therefore Eq. (4) is implicit. The displacements $\mathbf{d}_{i+1}$ can be written in terms of the predictor displacements $\hat{\mathbf{d}}_i$ (representing the explicit terms in Eq. (4)) and the remaining implicit terms in Eq. (4), where:

$$\mathbf{d}_{i+1} = \hat{\mathbf{d}}_{i+1} - (\Delta t)^2\beta\overline{\mathbf{M}}^{-1}(1+\alpha)\mathbf{r}_{i+1} \tag{5}$$

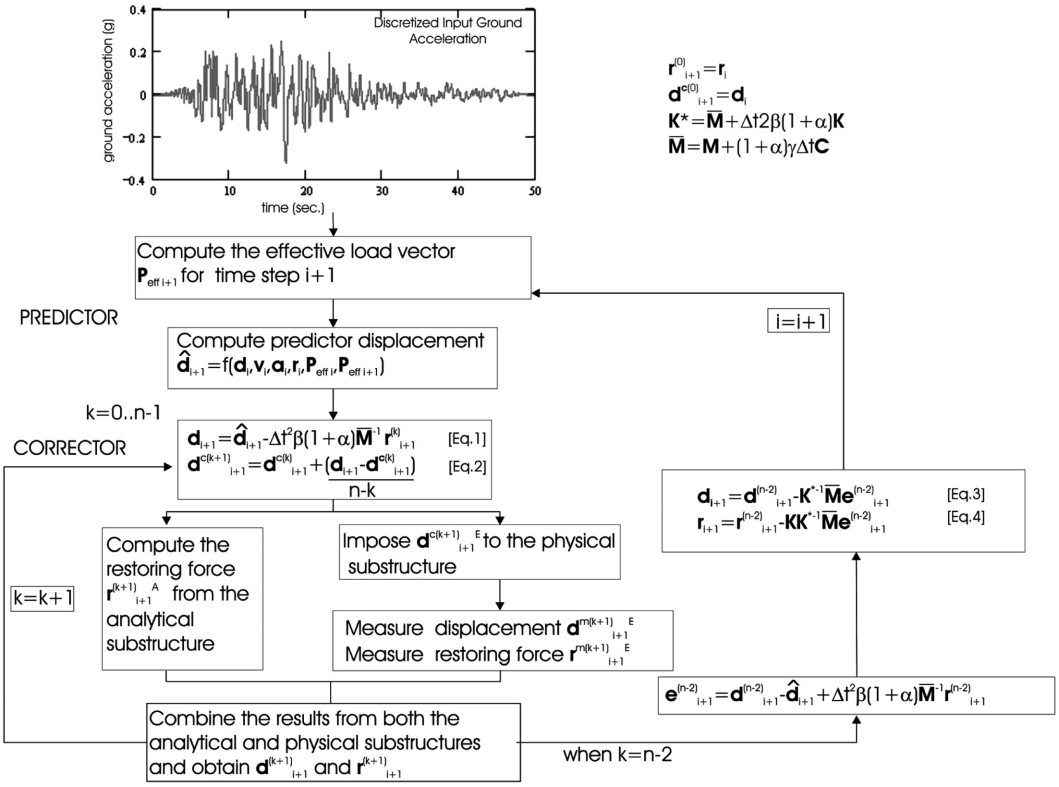

Fig. 4 α-method integration algorithm for real-time hybrid testing

Using the equations derived above, Shing, *et al*. (2002) developed an integration scheme for real-time pseudo-dynamic testing by introducing an iterative solution method that does not require slowing down or stopping the actuators at the end of a time step. The method is illustrated in Fig. 4, where first the predictor displacements $\hat{\mathbf{d}}_{i+1}$ for the next command displacements are computed from Eq. (4). The algorithm then proceeds with a correction using a fixed number of iteration cycles. Using Eq. (5) (also appearing as Eq. 1 in Fig. 4), the command displacements $\mathbf{d}_{i+1}$ are computed. For the first iteration cycle, in Eq. (5) the corrected restoring forces computed during the final iteration of the prior time step is used as $\mathbf{r}_{i+1}$ (see Eq. 4 in Fig. 4). In the correction phase, the computed target displacements $\mathbf{d}^{c(k+1)}{}_{i+1}$ that are imposed to the structure during iteration k is:

$$\mathbf{d}_{i+1}^{c(k+1)} = \mathbf{d}_{i+1}^{c(k)} + \frac{(\mathbf{d}_{i+1} - \mathbf{d}_{i+1}^{c(k)})}{n-k} \tag{6}$$

In Eq. (6) (also appearing as Eq. 2 in Fig. 4) n is the total number of fixed iterations, k is the iteration index, and c designates the calculated target command displacements. In the second term of Eq. (6), (n - k) is in the denominator, where as noted n is fixed and k increases as the iteration cycles proceed. The use of Eq. (6) leads to a more or less uniform incremental correction for the command displacements $\mathbf{d}^{c(k)}{}_{i+1}$. A conventional Newton iteration method during the correction phase would lead to decreasing incremental corrections as the solution converges to the exact values. This is not desirable for real-time testing, because either the actuators have to slow down or signals have to be sent to the actuator

controller at an increasing speed.

In Fig. 4, $\mathbf{r}^{m(k+1)}{}_{i+1}{}^{E}$ and $\mathbf{r}^{(k+1)}{}_{i+1}{}^{A}$ are the measured restoring forces from the test structure and analytical substructure restoring forces, respectively, that result from $\mathbf{d}^{c(k+1)}{}_{i+1}$ and which combine to form the restoring force $\mathbf{r}^{(k+1)}{}_{i+1}$ for the entire structure at the end of the k+1 iteration cycle. A convergence error after the $(n\text{-}1)^{th}$ cycle of iteration is defined as:

$$\mathbf{e}_{i+1}^{(n-2)} = \mathbf{d}_{i+1}^{(n-2)} - \hat{\mathbf{d}}_{i+1}(\Delta t)^2 \beta(1+\alpha)\overline{\mathbf{M}}^{-1}\mathbf{r}_{i+1}^{(n-2)} \tag{7}$$

which is used to correct for errors in the displacements $\mathbf{d}_{i+1}$ and restoring forces $\mathbf{r}_{i+1}$ based on equilibrium and information at the $(n\text{-}2)^{th}$ iteration step, see Fig. 4. By performing this equilibrium correction to eliminate convergence errors, the displacements and restoring forces are made available for the calculation of the predictor displacements $\hat{\mathbf{d}}_{i+1}$ for the next time step while the actuators are imposing the displacements during the last iteration substep n. As a result, the structure continues to be loaded in real time without any pause.

The above procedure is similar to one developed by Shing, *et al*. (2002), except that the computed target displacement $\mathbf{d}^{c(k)}{}_{i+1}$ is used in lieu of the measured displacement of the actuator in the second term of Eq. (6). Mercan (2007) determined that this modification improved the accuracy of the testing algorithm.

The α-method using a corrector with a fixed number of iteration cycles requires minimal computational effort for each iteration. As a result, the actuators can receive uninterrupted commands at fixed time intervals, and a continuous actuator motion with a more or less constant speed is provided. The method is an unconditionally stable implicit scheme, which is an advantage when a large number of degrees of freedom (DOFs) exist in the test. The correction scheme provided at the end of the time step is proven to be effective in eliminating spurious higher-mode response that could otherwise be introduced by experimental errors (Shing, *et al*. 1991).

A communication delay of 1/1024 sec. is present in the RTMD integrated control system, as noted above. Also, the dynamics of the servo-hydraulic test structure system introduces additional delay. Because of time delay or time lag, the measured restoring force that is fed back from the test structure does not correspond to the desired position (it is measured before the actuator has reached its target position). The effect of a time delay error is to introduce energy into the system, which may cause the test to go unstable (Horiuchi, *et al*. 1996, Mercan and Ricles 2007). Studies by Mercan (2007) indicate that the magnitude of the time delay in the restoring forces from the test structure and analytical substructure(s) that causes instability in the system depends on a number of items, including: (1) the amount of damping in the structural system; (2) the energy dissipation due to test structure inelastic deformations; (3) the number of degrees of freedom in the structural system; and (4) the proportion and magnitude of the time delay of the restoring force measured in a test structure relative to the restoring force determined by the analytical substructure at a degree of freedom (e.g. at the interface of the test structure and analytical substructure(s)). To minimize delays due to actuator dynamics, a feed forward component is added to the servo-control to maintain accurate control of the actuator. The feed forward component is discussed more in detail later.

4. Real-time hybrid test MDOF steel frame with elastomeric dampers

The three story moment resisting frame (MRF) shown in Fig. 5 was the focus of a series of real-time hybrid tests. The properties of the MRF without the dampers are summarized in Tables 1 and 2. The

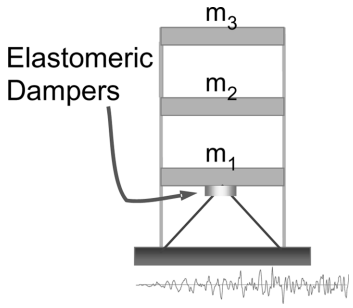

Fig. 5 Three-story MRF with elastomeric damper

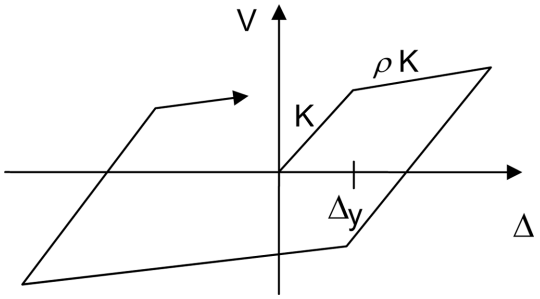

Fig. 6 Story shear-drift (V-Δ) relationship for MRF

damping matrix for the MRF was based on Rayleigh proportional damping, with a damping ratio of 0.02 in modes 1 and 3. Each story has the hysteretic behavior shown in Fig. 6, where the initial yield story drift Δ_y is equal to 10 mm and the strain hardening ratio ρ is equal to 0.015. As a means to reduce the seismic response of the MRF, elastomeric dampers are placed in the first story, as shown in Fig. 5. Each damper consists of three steel tubes, each tube containing a Butyl blend of rubber that is placed around a longitudinal steel bar and compressed inside the steel tube, see Fig. 7(a) and (b), where it is held in place by friction. The three tubes with the compressed elastomer are placed side by side, as shown in Fig. 7(c), and welded together by transverse bars. The damper has the characteristics of an elastomeric material at small deformation amplitudes (of less than 15 mm), with friction dominating the

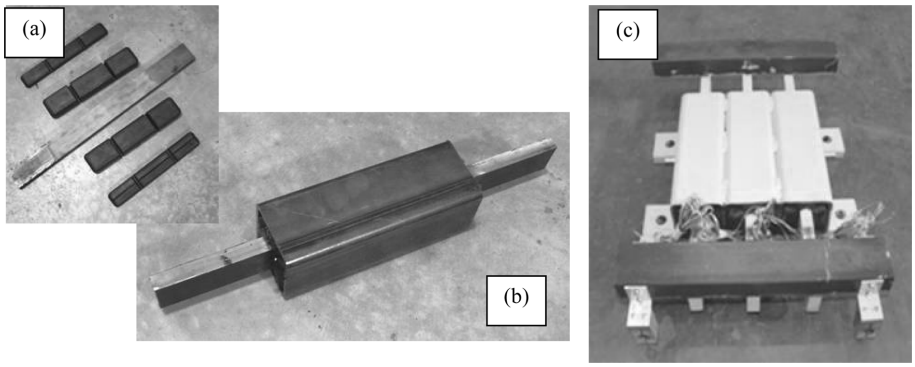

Fig. 7 Elastomeric damper: (a) steel bar and elastomer; (b) compressed inside a steel tube, and (c) assembled

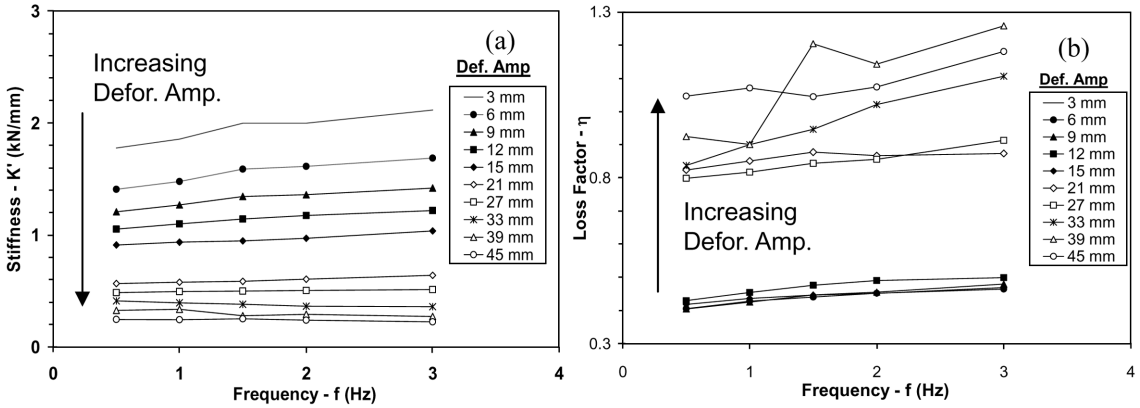

Fig. 8 Elastomeric damper mechanical properties for (a) stiffness K', and (b) loss factor at room temperature

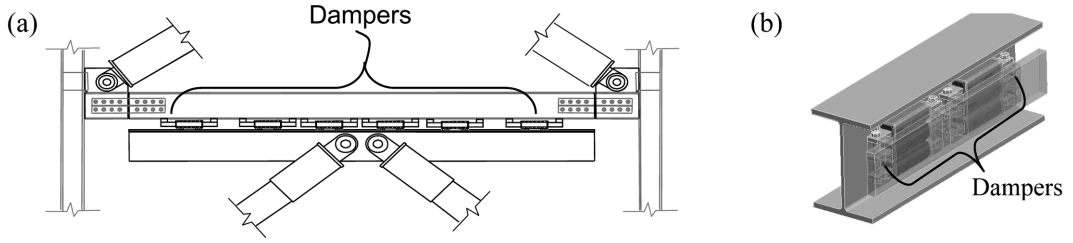

Fig. 9 Elastomeric damper installation detail: (a) beam bottom flange; (b) beam web

behavior at larger amplitudes. Material characterization tests on the damper were performed by Kontopanos (2006). The stiffness K' and loss factor η of the material as a function of excitation frequency and deformation amplitude are shown in Fig. 8. K' is the secant stiffness of the damper corresponding to the maximum deformation within a hysteretic loop developed under a constant amplitude of imposed deformation. The loss factor η is related to the energy dissipation of the damper per cycle of deformation. The stiffness K' is shown in Fig. 8(a) to be more frequency dependent at small deformation amplitudes than when larger deformations are imposed on the damper. The loss factor is shown in Fig. 8(b) to be frequency dependent, ranging from 0.4 to 0.5 at small deformations, with a significant increase in η at larger deformations to a value of 1.2 due to the frictional effects. The elastomeric damper is installed in a structure as shown in Fig. 9, where several are placed together to meet the design requirements, and are attached to either the flange or web of the beam.

The hybrid test involved three degrees of freedom, each associated with the horizontal displacement at a floor (see Fig. 10(a)). The moment resisting frame was modeled analytically, and was the analytical substructure for the hybrid test shown in Fig. 10(b). The dampers and lateral braces that formed the test structure are shown in Fig. 10(c). The analytical substructure was modeled using the properties in Tables 1 and 2 and SIMULINK (2007), and the numerical simulation model for the analytical substructure was placed on the Simulation Workstation shown in Fig. 3. The test setup for the test structure is shown in Fig. 11. The damper construction detail with the attachment of a pair of dampers connected to the beam web (Fig. 9(b)) was used in the setup. One of the 1700 kN dynamic actuators described previously was used to impose the command deformations to the pair of dampers. The test setup included two reaction frames (South A-Frame and North A-Frame), as well as a loading stub. The

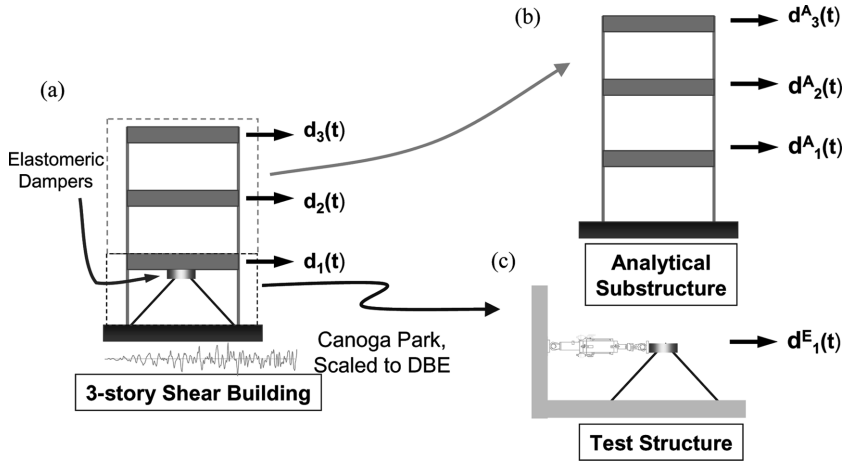

Fig. 10 Real-time hybrid test: (a) structural system; (b) analytical substructure, and (c) test structure

Table 1 MRF structural properties

Floor	Story Stiff. - K (kN/m)	Floor Mass - m (mtons)	Yield Drift- Δ_y (mm)	Strain Hardening - ρ
1	11760	135.5	10	0.015
2	11760	135.5	10	0.015
3	9800	67.8	10	0.015

Table 2 MRF elastic undamped modal properties

Mode	Period - T (sec)	Viscous Damping - ζ
1	1.31	0.02
2	0.49	0.018
3	0.37	0.02

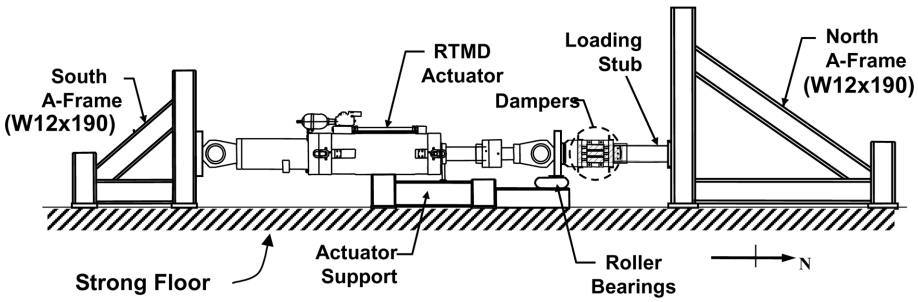

Fig. 11 Test setup

stiffness of the loading stub and North A-Frame was comparable to that of the diagonal bracing in the structure, and there was no need to include the diagonal bracing in the test setup. A photograph of the test setup and close-up of the damper is given in Fig. 12(a) and (b). Fig. 12(b) shows the pair of dampers attached to each side of a vertical plate representing the web of the first floor beam of the MRF.

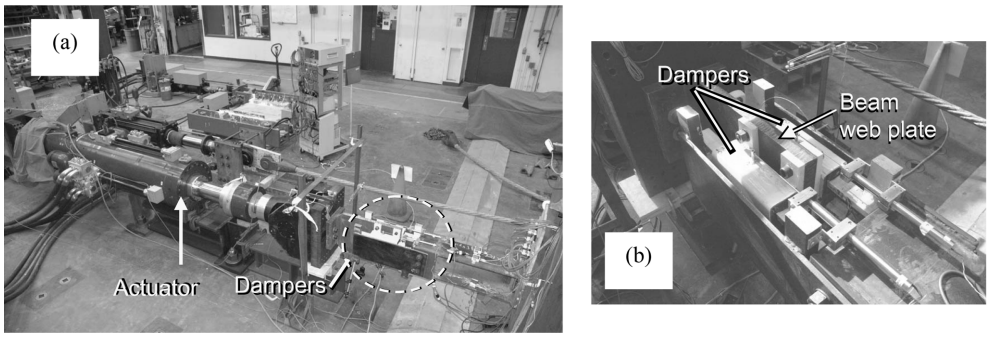

Fig. 12 Photographs of (a) test setup, and (b) close-up of dampers

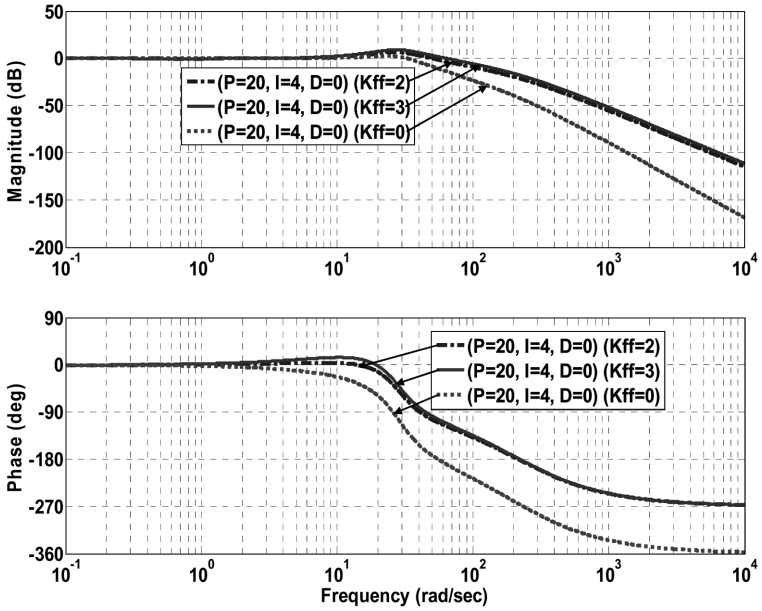

Fig. 13 Bode Diagram for the servo-hydraulic test structure system

For the hybrid test, the time step Δt was 0.0195 sec., with 20 correction substeps (i.e. $n = 20$) used in the integration algorithm explained above. Hence one controller clock tick occurs during each correction substep. Values of -0.0833, 0.2934, and 0.5833 were used for the integration parameters α, β, and γ, respectively. These values for the integration parameters are based on the recommendations of Hilber, *et al*. (1977) that were discussed previously in this paper, where the value for α of -0.0833 is equivalent to -1/12, and the same value that has been utilized by Shing, *et al*. (2002) in real-time testing. The structure was subjected to the N196E component of the 1994 Northridge earthquake ground motion recorded at Canoga Park, scaled to the Design Basis Earthquake (DBE) as defined in FEMA (2003), and in accordance with the procedure recommended by Somerville, *et al*. (1997). The servo-control law consisted of a PID control, with a velocity feed forward component. The control gains for position error (P), integral error (I) and derivative error (D) were 20, 4, and 0, respectively, and 2 for the control gain K_{FF} for the feed forward component. The control gains were established with the aid of the Bode diagram for the servo-hydraulic test structure system. Fig. 13 shows the Bode diagram, where

magnitude and phase plots for cases where control gains for the PID controller of $P = 20$ $I = 4$, and $D = 0$ are shown for various feed forward component control gains of $K_{FF} = 0$, 2, and 3. The adequacy of the control gains were verified using numerical simulations, where the servo-hydraulic system and structure were modeled in SIMULINK. The model for the servo-hydraulic system was developed using properties obtained from system identification tests by Zhang, *et al*. (2005). As a basis of comparison, real-time tests were performed with and without a feed forward component, and the resulting actuator tracking from the tests are compared.

5. Real-time hybrid test results

A numerical simulation of the structure without the dampers (i.e. hybrid test without the test structure) was initially performed. The first floor lateral displacement time history is shown in Fig. 14, where it is identified as Undamped Frame. The structure yielded as the first floor displacement d_1 exceeded 10 mm, and d_1 had a maximum magnitude of 55 mm. As a result of inelastic deformations in the structure, the MRF first story developed a permanent drift at the end of the earthquake, where the permanent displacement for d_1 was about 30 mm (note that the first story drift is equivalent to the displacement d_1). The test results for the MRF with the elastomeric dampers, where a feed forward component control gain of K_{FF} of 2 was used, is also given in Fig. 14, where it is identified as Damped

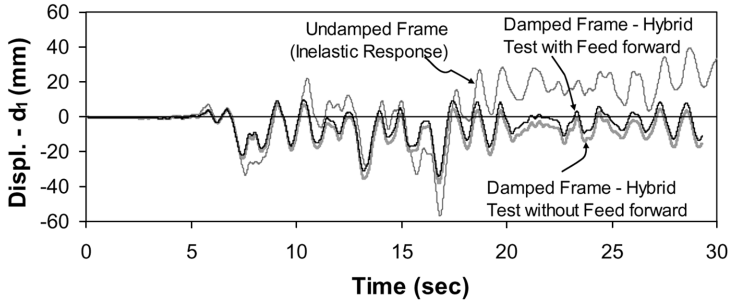

Fig. 14 First floor displacement time history test with and without feed forward control, and comparison with and mped frame response

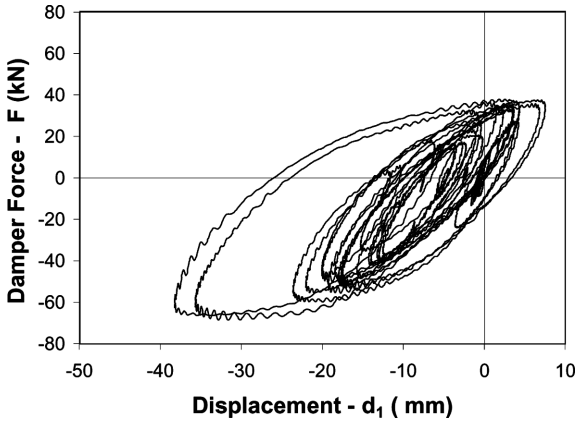

Fig. 15 Damper hysteretic response, real-time

Frame – Hybrid Test with Feed forward. The hybrid test with the dampers in the test structure resulted in a maximum displacement for d_1 of 32 mm, where again yielding developed in the first story. The force-deformation behavior for the pair of dampers is shown in Fig. 15. Energy dissipation is seen to occur, where at a smaller deformation the damper response resembled that of a visco-elastic damper (i.e., the hysteresis loops were elliptical shaped), while at larger deformations (beyond a magnitude of 15 mm) slip occurred and additional energy was dissipated by friction. The slip was not significant, as the dampers nearly self-centered and a permanent drift of 3 mm occurred in the first story following the test.

The success of a real-time test depends on minimizing any delay in the restoring force that is fed back to the integration algorithm, while achieving the target displacement of the actuator within the time step. As noted above, the communication between the Simulation Workstation and the Controller Workstation causes a delay of one clock tick (1/1024 sec.). The use of the above PID settings and feed forward component control gain of 2 resulted in exceptional tracking by the hydraulic actuator, and the imposed displacement by the actuator lagged behind the command displacement by only one clock tick. Hence, a total delay of two clock ticks existed in the system, where the measured component of the restoring force **r** from the test structure used in the integration algorithm on the Simulation Workstation had a two clock tick delay, while the restoring force from the analytical substructure had no delay since its numerical simulation model resided on the Simulation Workstation. With the same PID settings and no feed forward component, the imposed displacement by the actuator lagged behind the command displacement by 27 clock ticks (27/1024 sec.), resulting in a total delay of 28 clock ticks in the measured restoring force and displacement. The result of omitting the feed forward component in the servo-hydraulic control on the hybrid test can be seen in Fig. 14, where the time history for d_1 (identified as Damped Frame – Hybrid Test without Feed forward) is compared with that from the hybrid test with the feed forward component. The test without the feed forward component had a maximum displacement magnitude of 37 mm, and a 5 mm maximum discrepancy from the results with the feed forward component. The discrepancy between the two results becomes larger as the MRF developed inelastic response. While the time delay of 28 clock ticks is considered significant because it affects the accuracy of the hybrid test, it did not cause instability in the test because of the damping present in the system from the elastomeric dampers and energy dissipation of the MRF.

In real-time hybrid testing, the quality of the results, assuming no time delay in the analytical substructure restoring force, is best judged by examining the tracking of the hydraulic actuator (Mercan 2007). A tracking indicator was developed by Mercan (2007) for this purpose. The tracking indicator, TI, is based on the enclosed area of any hysteresis in the synchronized subspace plot, where the actuator command displacement d^c is plotted against the measured actuator displacement d^m. The TI was computed at each time step during the test using Eq. (8), where at time step i:

$$TI_i = 0.5(A_i - TA_i) \tag{8}$$

In Eq. (8) A_i and TA_i are equal to the enclosed area and complementary enclosed area, respectively, at time step i, where

$$A_i = A_{i-1} + 0.5(d^c_{i+1} + d^c_i)(d^m_{i+1} - d^m_i) \tag{9a}$$

$$TA_i = TA_{i-1} + 0.5(d^m_{i+1} + d^m_i)(d^c_{i+1} - d^c_i) \tag{9b}$$

At the beginning of the test, the initial values for A_i and TA_i are set equal to zero (i.e. $A_i = TA_i = 0$).

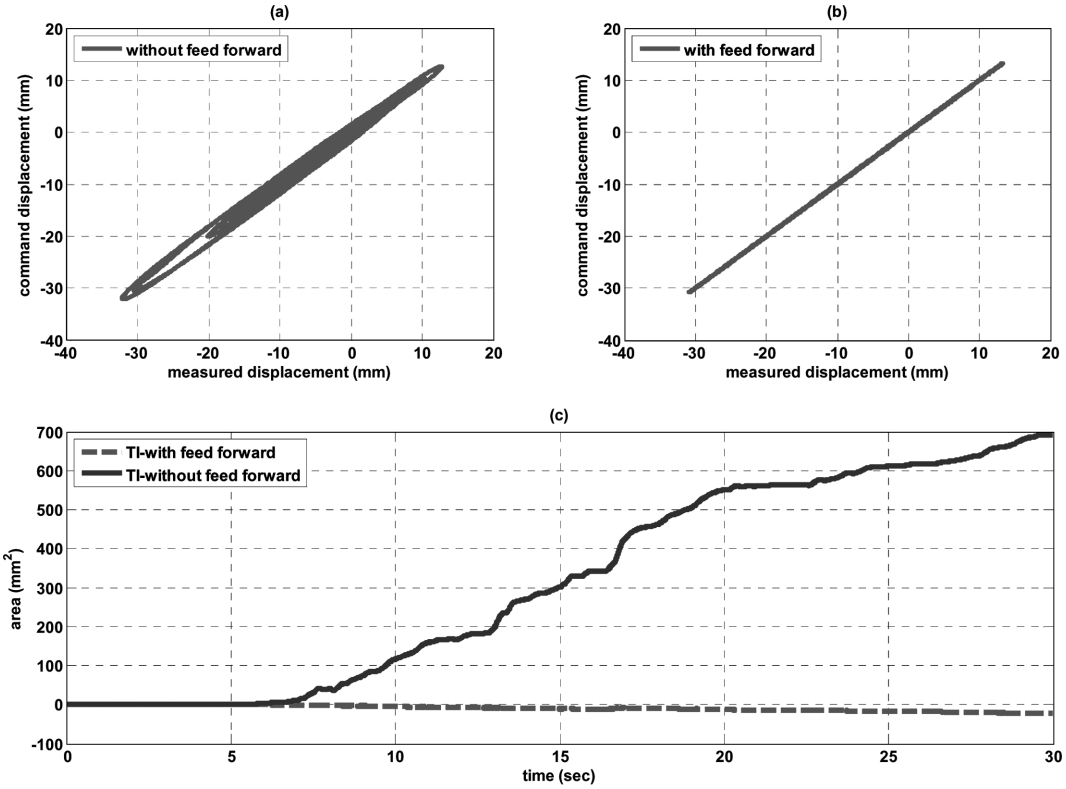

Fig. 16 Real-time hybrid tests results: synchronization subspace plots (a) without and (b) with feed forward control, and (c) tracking indicator

A positive slope for the TI implies that the measured displacement is lagging behind the command displacement, whereby energy is introduced into the system that cause inaccuracies in the test. A negative slope implies that the measured displacement is leading the command displacement, which adds damping into the system and also causes inaccuracies in the test. A zero slope implies no error associated with lead or delay, and the measured actuator displacements and the command displacements are in phase with respes to each other.

The synchronization subspace plot for the tests without and with the feed forward component is shown in Fig. 16(a) and (b), respectively. The TI's for both cases are shown in Fig. 16(c). The TI show that there is an actuator delay during the test without the feed forward component, where the positive slope for the indicator implies a time delay. The use of the feed forward component with a gain K_{FF} equal to 2 shows exceptional tracking by the servo-controlled actuator, where the slope for the corresponding TI in Fig. 16(c) is orders of magnitude smaller. On the basis of the values for the TI, the hybrid test with the feed forward component is considered to be significantly more accurate than the test without the feed forward component.

6. Determination of damper requirements to meet MRF seismic performance requirements

A performance-based design procedure involving the use of elastomeric dampers in steel frame

systems was developed by Lee, *et al*. (2005). The procedure involves selecting the target seismic performance and associated design criteria, and performing the damper design by considering a range of values for the damper stiffness relative to the frame lateral story stiffness and brace stiffness, as well as the structural characteristics of the frame (natural period, first mode shape, member forces resulting from seismic loading). Lee, *et al*. (2006) show that it is possible to economically design a steel frame with elastomeric dampers where the maximum drift is less that 1.5% and the members in the steel frame remain essentially elastic under the DBE ground motions. For the elastomeric dampers considered in this paper, the combined frictional and elastomeric behavior of the damper make it difficult to assign a value for K' and η for use in the procedure, since these properties are dependent upon deformation amplitude. If an accurate analytical model does not exist for the damper, an assessment of whether the dampers are effective in meeting the performance objectives of the design would not be reliable using a time history analysis.

The real-time hybrid testing method is ideal to evaluate structural performance under dynamic loading when the behavior of components of a structural system cannot be accurately modeled analytically. Consequently, the test method was utilized to determine the design requirements and to assess the effectiveness of the elastomeric dampers considered in this paper to enable the 3-story MRF to meet a selected performance objective. The selected performance objective required the MRF first story to remain elastic under the DBE ground motions. Considering the use of the elastomeric dampers described above, the number of dampers that would enable this performance objective to be met needed to be determined. To accomplish this, the existing test setup shown in Fig. 11 was used and the real-time hybrid testing algorithm was modified, where the measured restoring force $r^{m(k+1)E}_{i+1}$ (see Fig. 4) is multiplied by a factor λ to associate $r^{m(k+1)E}_{i+1}$ with representing the number of pairs of dampers being simulated in the structural system in the first story. By performing a series of real-time hybrid tests, each with a different value for λ, the number of pairs of dampers required to have the MRF remain elastic in the first floor could be determined. The as-built test setup represented the case where one pairs of dampers was used, where $\lambda = 1$.

Twelve real-time hybrid tests were performed, where the structural system was subjected to the same DBE-scaled ground motion at Canoga Park and λ varied from 0 (i.e. no dampers) to 7. The results for the first story drift as a function of the number of dampers are shown plotted in Fig. 17 for the twelve tests. With no dampers, the first story drift was 59 mm, closely agreeing with the time history analysis of the MRF without dampers. It was determined from the test results that seven dampers are required (i.e., $\lambda = 3.5$) in order to have the first story remain elastic. Since the dampers are placed in pairs, one on

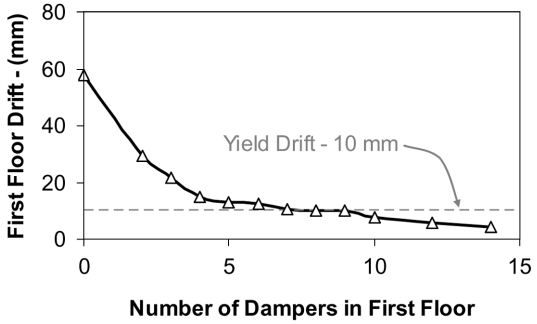

Fig. 17 First floor MRF drift results from real-time hybrid test series for various number of dampers (λ varying from 0 to 7)

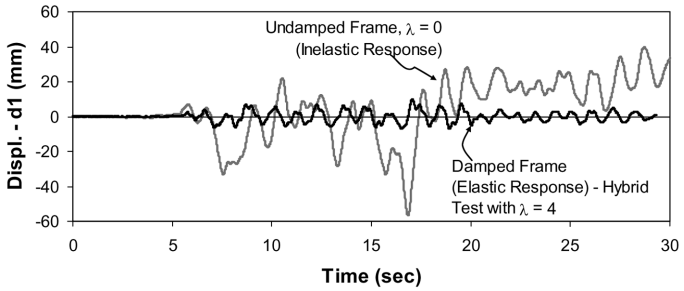

Fig. 18 First floor MRF displacement results from real-time hybrid test of undamped and damped structure with 8 dampers

each side of the beam web in the prototype structure, a total of four pairs of dampers (i.e. altogether 8 dampers, where $\lambda = 4$) are recommended. The time history of the first floor displacement from the test with $\lambda = 4$ is shown plotted in Fig. 18, where it is compared to the first floor displacement of the MRF without any dampers. Fig. 18 shows the maximum magnitude of displacement at the first floor is reduced to 10 mm in the frame with $\lambda = 4$.

7. Summary and conclusions

This paper described the NEES Real-time Multi-directional Earthquake Simulation Facility that has been constructed at Lehigh University. The servo-hydraulic components, the integrated control hardware and software, and the testing algorithms that exist at the facility enable real-time hybrid testing to be successfully performed. Real-time hybrid testing of a steel MRF with elastomeric dampers was presented, illustrating the ability of the facility to test complex structures in real time. The real-time hybrid test method was utilized to determine the effectiveness of complex elastomeric dampers, which are sensitive to both loading rate and deformation amplitude, in reducing potential seismic damage to the MRF under the design earthquake. A tracking indicator was developed to enable the tracking of an actuator during a test to be examined and enabled the quality of the test results to be assessed.

Ongoing work involving real-time hybrid testing at the RTMD facility include the performance evaluation of multi-story steel frame systems with elastomeric dampers. Several additional test setups, each with an individual dynamic actuator and pairs of dampers will be added to the current configuration that exist in order to perform real-time hybrid testing of multi-story buildings. The expanded setup will enable several parameters to be investigated, including location of damper placement over the height of the building as well as in the floor plan of the building.

Future research at the RTMD facility will involve real-time hybrid testing of structural systems with magnetorheological (MR) dampers, as well as other types of smart dampers and devices. The goal of this research is to acquire experimental data from large-scale tests, where realistic seismic demands are imposed and the interaction of the dampers or devices with the structural system is included. The data is to be utilized to improve existing analytical models and to develop new ones that enable accurate time history analysis of structural systems to be performed. In addition, the data is to be used to develop design procedures to enable smart dampers to be effectively utilized in seismic hazard mitigation of structural systems. A summary of current and recent research conducted at the RTMD facility appears on the facility's web site (*www.nees.lehigh.edu*).

Acknowledgments

This paper is based upon work supported by a grant from the Pennsylvania Department of Community and Economic Development through the Pennsylvania Infrastructure Technology Alliance. The research was performed at the Lehigh NEES equipment site, which is supported by the National Science Foundation (NSF) under Grant No. CMS-0402490 within the George E. Brown, Jr. Network for Earthquake Engineering Simulation Consortium Operation. Any opinions, findings, and conclusions or recommendations expressed in this material are those of the authors and do not necessarily reflect the views of the sponsor. The authors wish to thank Corry Rubber Company for donating the elastomeric dampers used in the research reported in this paper. In addition, the authors would like to express their appreciation to Robert Michaels and Shannon Sweeney of Penn State Erie for their development of the prototype damper used in the research reported in this paper.

References

Darby, A. P., Blakeborough, A. and Williams, M. S. (2001), "Improved control algorithm for real-time substructure testing", *Earthq. Eng. Struct. Dyn.*, **30**(3), 431-448.

Dermitzakis, S. N. and Mahin, S. A. (1985), "Development of substructuring techniques for on-line computer controlled seismic performance testing", *Report UBC/EERC-85/04,* Earthquake Engineering Research Center, University of California, Berkeley.

FEMA (2003), "NEHRP recommended provisions for new buildings and other structures, part 1 - provisions", Report No. FEMA 450, Federal Emergency Management Agency, Washington, D.C.

Hilber, H. M., Hughes, T. J. R. and Taylor, R. L., (1977), "Improved numerical dissipation for time integration algorithms in structural dynamics", *Earthq. Eng. Struct. Dyn.*, **5**, 283-292.

Horiuchi, T., Nakagawa, M., Sugano, M. and Konno, T. (1996), "Development of a real-time hybrid experimental system with actuator delay compensation", *Proceedings of the Eleventh World Conference on Earthq. Eng.,* Paper No. 660.

Kontopanos, A. (2006), "Experimental investigation of a prototype elastomeric structural damper", MS. Thesis, Lehigh University, Bethlehem, PA.

Lee, K., Ricles, J. and R. Sause. (2006), "Performance based seismic design of steel MRFs with elastomeric dampers, *J. Structural Eng.*, submitted for publication.

Lee, K.-S., Fan, C.-P., Sause, R., and Ricles, J. (2005), Simplified design procedure for frame buildings with viscoelastic or elastomeric dampers, *J. Earthq. Eng. Struct. Dyn.*, **34**, 1271-1284.

Mazzoni, S., McKenna, F., Scott, M., and Fenves, G., (2006) "Open system for earthquake engineering simulation (opensees) user command language manual", Version 1.7.3, Pacific Earthquake Engineering Research Center, University of California, Berkeley.

Mercan, O. (2007), "Analytical and experimental studies on large-scale, real-time pseudodynamic testing", Ph.D. Dissertation, Lehigh University, Bethlehem, PA.

Mercan, O. and Ricles, J. M. (2007), "Stability and accuracy analysis of outer loop dynamics in real-time pseudo-dynamic testing of SDOF systems", *Earthq. Eng. Struct. Dyn.*, accepted for publication.

Mercan, O. and Ricles, J. M. (2005), "Evaluation of real-time pseudodynamic testing algorithms for seismic testing of structural assemblages", *ATLSS Report No. 05-06*. Center for Advanced Technology for Large Structural Systems, Lehigh University, Bethlehem, PA.

Nakashima, M. and Masaoka N. (1999), "Real-time on-line test for MDOF systems", *Earthq. Eng. Struct. Dyn.*, **28**, 392-420.

Nakashima, M., Kato, H. and Takaoka, E. (1992), "Development of real-time pseudodynamic testing", *Earthq. Eng. Struct. Dyn.*, **21**, 79-92.

NEES Cyberinfrastructure Center (2007a), "Flexible telepresence system", FlexTPS 2.2 User's Guide, http://it.nees.org/software/flextps/index.php, La Jolla, CA.

NEES Cyberinfrastructure Center (2007b), "Getting started data turbine 3.7", http://it.nees.org/software/dataturbine/index.php, La Jolla, CA.

NEES Cyberinfrastructure Center (2007c), "Real-time data viewer", RTV 1.5 User's Guide, http://it.nees.org/software/rdv/index.php, La Jolla, CA.

Newmark, N. N. (1959), "A method of computation for structural dynamics", *J. Eng. Mech. Div. ASCE*, **85**, 67-94.

Shing, P. B., Wei, Z., Jung, R. Y. and Stauffer, E. (2004), "NEES fast hybrid test system at the University of Colorado", *Proceedings of the 13th World Conference on Earthquake Engineering*, Vancouver, Canada, Paper No. 3497.

Shing, P. B., Spacone, E. and Stauffer, E. (2002), "Conceptual design of fast hybrid test system at the University of Colorado", *Proceedings of the 7th U.S. National Conference on Earthquake Engineering*, Boston, Massachusetts.

Shing, P. B. and Vannan, M. T. and Cater, E. (1991), "Implicit time integration for pseudodynamic tests", *Earthq. Eng. Struct. Dyn.*, **20**, 551-576.

Simulink (2007), The Math Works, Inc., Natick, Massachusetts.

Somerville, P., Smith, N., Punyamurthula, S. and J. Sun. (1997), "Development of ground motion time histories for phase 2 of the FEMA/SAC steel project", *SAC Background Doc. SAC/BD-97/04*, SAC Jt. Venture, Sacramento, CA.

Zhang, X. P., Ricles, J. M., Mercan, O. and C. Chen. (2005), "Servo-hydraulic system identification for the NEES real-time multi-directional earthquake simulation facility", *ATLSS Report No. 05-14*, Center for Advanced Technology for Large Structural Systems, Lehigh University, Bethlehem, PA.